



**Deliverable Report for Grant Agreement Number 760813**

**Deliverable 6.2**

## ***In vitro* dosimetry modelling and experimental design report**

**Due date of deliverable: 30<sup>th</sup> September 2020**  
**Actual submission date: 21<sup>st</sup> September 2020**

**Lead beneficiary for this deliverable: *IOM***

<b>Dissemination Level:</b>		
PU	Public	X
PP	Restricted to other programme participants (including the Commission Services)	
RE	Restricted to a group specified by the consortium (including the Commission Services)	
CO	Confidential, only for members of the consortium (including the Commission Services)	

**TABLE OF CONTENTS**

<b>1. Description of task</b>	<b>3</b>
<b>2. Description of work &amp; main achievements</b>	<b>5</b>
<b>3. Deviations from the Workplan</b>	<b>27</b>
<b>4. Performance of the partners</b>	<b>27</b>
<b>5. Conclusions</b>	<b>27</b>
<b>6. Annex:</b>	<b>28</b>

## 1. Description of task

### Task 6.2 *In vitro* dosimetry modelling and experimental design; (IOM, Harvard, QSAR Lab, UNIPI, UNamur, RIVM); M1-33

The T6.2 partners (led by IOM) held a workshop for design of the WP1, 3, 4 *in vitro* experiments at the kick off meeting. The outcomes of this workshop were a dosing regimen for each tested engineered nanomaterial (ENM) in each *in vitro* system and SOPs for setting up experiments normalised or referenced to cell density and the physiological model under consideration. This workshop was organised by IOM in close collaboration with Harvard. During the first quarter, four models will be developed or used: a QSAR model (QSAR Lab), an ENM deposition model (RIVM), a scaling and fluidic model and an *in vitro* kinetics model (UNIPI).

Specifically,

1. QSAR modelling was carried out, post-processing, (QSAR Lab, UNamur) to construct a relationship between ENM physico-chemical characteristics with the biological responses and design criteria, using the existing data from earlier projects (e.g. MARINA, SUN, NANOSOLUTIONS) – now, part of the PATROLS database. Later, when PATROLS data become available, they will be used to validate the QSAR model predictions.
2. The multiple path particle dosimetry (MPPD) model calculates the deposition fraction of inhaled particles in the different region of the experimental animals (including rat) and human (age 3 month up to adult) lung using the particle physico-chemical characteristics, the respiratory tract architecture, the physiological breathing pattern. The MPPD model is already been developed, user-friendly MPPD software that is available free to the public and used in many EU nanosafety projects. MPPD calculates deposition and clearance simultaneously for up to four lognormal distributions. In PATROLS, the model will be used to calculate the deposited dose in different regions of the lung for the chosen ENM. Partners in this task have close connections with the developers of the model should adjustments be needed.
3. The fluidic model is a mathematical representation of the fluidic bioreactor prototypes of WP3 and 4 and is used to inform their design and construction. The model is parameterised for different bioreactor heights (for identification of optimum basal compartment height which ensures adequate oxygen and optimum apical compartment height for uniform particle deposition), pneumatic pressures (for determining membrane deformation according to its elastic properties and the amount of media to displace) and media flow rates (for shear stress calculations, which are necessary to minimize cell damage). The model helps in determining

the optimal size for the lung model device to ensure it is easy to manage under a hood and in an incubator and still has a sufficiently small media height to ensure a physiological lung oxygen supply but with a sufficient height to allow uniform ENM aerosol deposition. To implement model simulations CFD (computational fluid dynamics) is coupled with mass and energy transport to determine the oxygen concentration and average temperature on the apical and basal side of the bioreactor. For the WP3 bioreactor, we simulate the formation and deposition of a ENM cloud (i.e. aerosol) on a membrane using multiphase modelling. Moreover, we will use FSI (fluid-structure interaction) to evaluate the motion of the flexing membrane as a function of applied pressure. Furthermore, to aid experimentalists in designing more realistic biomimetic *in vitro* systems, UNIFI also develops allometry-scaling based design criteria such that *in vitro* experiments recapitulate quarter power “metabolically-supported functional scaling”. These criteria, specifically cell density and the size of 3D constructs developed in WP3 and 4, are used as a baseline by experimentalists to design cell culture systems.

4. In FP7 SUN, a kinetics model was developed by IOM to describe the dose-response in simple *in vitro* models. The model describes the distribution of the deposited dose into the *in vitro* cell population. IOM will further adapt this model for the more sophisticated *in vitro* models developed in PATROLS with several interacting cell populations. UNIFI simulated the deposition of ENM in these physiologically relevant *in vitro* environments using their published model which will help in calculating the exact dose interacting with the cells. A graphical user interface (GUI) will be constructed by UNIFI (originally planned by IOM) as user-friendly front end to the Harvard model to facilitate its use by the experimental partners. The benchmark dose approach will also be carried out, by RIVM, in parallel for comparison.

## 2. Description of work & main achievements

### 2.1 QSAR Modelling

To date, in collaboration with Dr. Sabina Halappanavar (Health Canada) and Prof. Ulla Vogel (National Research Centre for the Working Environment) we have proposed and verified the application of the novel transcriptomic-based and AOP-informed Nano-QSAR model.<sup>[1]</sup> This approach makes use of 1) an AOP established for lung fibrosis (an AO of relevance to nanomaterials), clearly identifying the key biological events essential for the initiation and manifestation of lung fibrosis ([www.aopwiki.org/aops/173](http://www.aopwiki.org/aops/173)) to rationalize and select the upstream biological event; 2) perturbations in transcriptomics pathways (as opposed to traditionally used expression changes in single or multiple gene targets) as endpoints targeting the selected upstream KE, and 3) carbon nanotubes (CNTs) as model nanomaterials that are shown to cause lung fibrosis in experimental rodent models, to identify the specific structural features of CNTs that are responsible for triggering part of the fibrosis mechanism.

In our approach, we have used the genome-wide transcriptomic profiles of lungs of mice exposed to 10 different multi-walled carbon nanotubes (MWCNTs).<sup>[2,3]</sup> The high-content gene expression data were analysed using statistical and bioinformatics tools to identify specific pathways perturbed following exposure. Benchmark dose (BMD) analysis was conducted to sort the pathways that show dose-response and to identify the most sensitive pathways with lowest BMD values.<sup>[4]</sup> Of several different pathways showing dose-response, three individual pathways were selected based on 1) pathways with the lowest BMD values, 2) pathways that are associated with the KEs of AOP 173 and more importantly, 3) pathways that are consistently perturbed across all 10 MWCNTs investigated. The statistical lower bound of the pathway BMD estimates (BMDL) for the selected pathways was derived and used as endpoint values in both supervised as well as unsupervised techniques aimed to link the structural characteristics of MWCNTs with the pathway level dose response.

As a result, we have developed a Nano-QSAR model describing quantitatively the relationship between the BMDL values of the ‘Agranulocyte adhesion and diapedesis’ pathway (BMDL<sub>AA</sub>) and the aspect ratio of MWCNTs:

$$\text{BMDL}_{AA} = 15.07 - 0.07 \kappa \quad (1)$$

$$R^2 = 0.86; \text{RMSE}_C = 1.63; Q^2_{\text{EXT}} = 0.62; \text{RMSE}_{\text{EXT}} = 2.34$$

where:  $R^2$  was the correlation coefficient between the predicted and observed values of BMDL, calculated for the training set;  $RMSE_C$  – the root mean square error of calibration (with training set);  $Q^2_{EXT}$  – the validation coefficient calculated for the validation set;  $RMSE_{EXT}$  – the root mean square error of validation (with validation set). The results indicated that an increasing aspect-ratio caused a decrease of the BMDL values, which suggest that high-aspect ratio nanotubes influence process of inflammation stronger than short MWCNTs.

In order to better understand the mode of inflammation response induced by MWCNTs we have performed comprehensive analyses of gene expression profiles associated with ‘Agranulocyte adhesion and diapedesis’ with the application of the Principal Component Analysis. The results indicate that mode of inflammation is different in case of the high-aspect ratio and entangled nanotubes and this is related to differences in perturbation of genes significant for the PC2: genes coding selectins, myosins and chemokines.

The results revealed that the aspect ratio ( $\kappa$ ) of MWCNTs can be used as a predictor of the biological event that initiates the inflammation process described by the ‘Agranulocyte adhesion and diapedesis’ pathway. The results also showed that while all MWCNTs are able to mount an acute and robust inflammatory response, which may potentially be detrimental when unresolved, impeding the ability to mount such response by competitively binding the regulatory molecules involved in the inflammatory process and failure to remove the impending danger in a timely manner, can also prove detrimental.

Within the PATROLS project, the novelty of the proposed transcriptomic-based and AOP-informed Nano-QSAR model is that the variance in the pathway dose-response is predicted purely from the variance in the structures of the modelled MWCNTs. Moreover, in this novel approach information derived from the AOP framework has been used to select the endpoint data to be modelled within the Nano-QSAR method. Thus, the relevance of the modelled endpoint to the possible adverse outcome at the organism level can be properly justified. This newly proposed AOP-informed methodology of building predictive models creates an opportunity to develop a modern computational nanotoxicology paradigm that is based on a sound mechanistic basis. It is a valuable step forward in effective determination of the structural features of nanomaterials that can be detrimental in the context of analysed adverse outcome and enabling testing of a diverse set of materials in a timely manner.

Summing up, we have demonstrated the high potential of the new approach, AOP-informed Nano-QSAR. The results of the study may serve as proof-of-concept for further development of the framework that combines the concepts of Nano-QSAR and Nano-AOP for better

understanding and predicting the adverse effects of nanomaterials on human health and form the basis for comprehensive and realistic risk assessment.

These results attracted great interest and enthusiastic feedback from researchers present at NanoAOP meeting of OECD WPMN, 16-18 December 2019, Paris, France.

## **2.2 The multiple path particle dosimetry (MPPD)**

The MPPD model was developed fully and is available in the public domain [1]. The model is used together with the *in vivo* kinetics model developed in D6.3 to estimate the deposited dose of NP in the different regions of the rat lung. The modelling of the bio-distribution of the NP in the lung and in secondary organs is currently being done in T6.3 and will be reported in D6.3.

## **2.3 The fluidic model - DosiGUI: a Graphical User Interface for ENM dosimetry**

### **Introduction**

Much uncertainty still remains regarding which constituent (*e.g.* nanoparticles (NPs) or dissolved ions) mainly contributes to the cellular toxicity of nanomaterials [1] - [3]. In this light, standardized experimental methodologies [4], [5] and computational approaches [6] - [8] simulating nanoparticle (NP) dynamics in liquid media have been provided to perform a more accurate dose-response analysis [9], [10]. Among them, the best known *in silico* tools are the ISDD (*In vitro* Sedimentation, Diffusion and Dosimetry) model [7], its extension ISD3 (which also includes Dissolution) [18] and the DG (Distorted Grid) model [6].

A graphical user interface (GUI) was developed at UNIFI for comparing the three nanodosimetry models, with the aim to identify the most suitable one for a specific application and to exploit it for accurately predicting the dose effectively delivered to tissues and cells. The rationale is to promote integrated *in vitro-in silico* approaches for better interpreting cytotoxicity effects induced by the exposure to nanomaterials, minimizing time-consuming, expensive and ethically sensitive *in vivo* tests [10].

### **Materials and methods**

The ISDD, DG and ISD3 models are able to describe one-dimensional (1D) NP dynamics in liquid media (Fig.1).

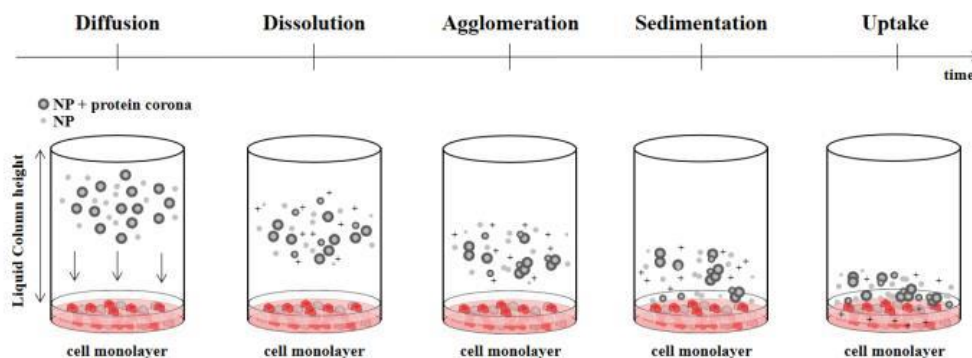


**Fig. 1:** NP dynamics in liquid media over time (adapted from [8],[10]).

#### A. In vitro Sedimentation, Diffusion and Dosimetry (ISDD) model

The ISDD model reproduces dosimetry of non-interacting spherical particles and agglomerates in monolayer cell culture systems [7]. It applies well established principles of diffusive and gravitational transport of particles in viscous media to calculate the movement of NPs from the medium bulk to the bottom of a vessel where cells reside. This model further produces a time-course of NP surface area, number and mass transported to the bottom of the vessel, without accounting for NP uptake by the cells. The fraction of NPs, their surface area, mass and number reaching cells, as well as the Area Under the Time-Delivered Dose Curve (AUC), are finally reported.

#### B. Distorted Grid (DG) model

The DG model computes diffusion and sedimentation of NPs in liquid media over time. Compared to ISDD, DG additionally models the dissolution process as a simple reduction of the agglomerate sizes over time. In DG, the bottom of the experimental set-up is characterized by a tuneable stickiness, describing the different possible levels of affinity between NPs and cells, and ranging from a purely reflective boundary condition (*i.e.* no NP uptake by the cells) to a totally sticky one (*i.e.* all NPs reaching the monolayer are immediately adsorbed and exit from the solution). The DG model finally provides concentration and deposition outputs in terms of number of NPs and nanomaterial surface area [6].

#### C. In vitro Sedimentation, Diffusion, Dissolution and Dosimetry (ISD3) model

The ISD3 model provides a general modelling framework for soluble NPs, adaptable to a wide range of experimental conditions, NP types and approaches for describing sedimentation and dissolution [8].

Dissolution can also be turned off, rendering a model like ISDD [17]. Unlike DG, ISD3 assumes a binary condition for the set-up bottom, according to which NPs can be instantaneously taken up by cells when reaching their surface and exit from the culture medium (sticky boundary condition) or alternatively meet a totally “impermeable” bottom (no flux boundary condition). Differently, cellular uptake of dissolved ions is explicitly modelled as a membrane diffusion process.

Table. 1 summarizes the NP dynamics modelled by each of the aforementioned models, comparing differences and similarities. Instead, the whole set of input parameters requested by each of the models is shown in Tab. 2.

*Table. 1: Comparison among the three models in terms of considered NP dynamics.*

		<i>In silico models</i>		
		<b>ISDD</b> (Hinderliter et al., 2010)	<b>DG</b> (DeLoid et al., 2015)	<b>ISD3</b> (Thomas et al., 2018)
NP dynamics	<b>Diffusion</b>	<b>Modelled</b>	<b>Modelled</b>	<b>Modelled</b>
	<b>Dissolution</b>	<b>Not Modelled</b>	<b>Not Modelled</b> (reduction in agglomerate size)	<b>Modelled</b> (free and protein-bound ions)
	<b>Agglomeration</b>	<b>Modelled</b> (single agglomerate size at time)	<b>Modelled</b> (high-resolution size distributions for polydispersity)	<b>Modelled</b> (particles with size greater than primary undissolved particle)
	<b>Accumulation</b>	<b>Modelled</b> (complete deposition on the bottom)	<b>Modelled</b> (deposition or cumulative dose adsorbed by cells)	<b>Modelled</b> (deposition or cumulative dose adsorbed by cells)
	<b>Instantaneous Cell Uptake</b>	<b>Not Modelled</b>	<b>Modelled</b> (adsorption tuned by means of the dissociation constant)	<b>Modelled</b> (total adsorption or no adsorption at all)

**Table. 2:** Comparison among the three models in terms of requested input parameters.

	<b>ISDD</b> (Hinderliter et al., 2010)	<b>DG</b> (DeLoid et al., 2015)	<b>ISD3</b> (Thomas et al., 2018)
<b>Liquid medium characteristics</b>	Dish depth [m], Volume [mL], Temperature [K] Viscosity [N s/m <sup>2</sup> ], Density [g/mL]		
<b>NP characteristics</b>	Hydrodynamic diameter [nm]		
		Diameters and fractions of each existing NP species [nm]	
<b>Protein-coated NP characteristics</b>	Effective density [g/mL]		
			Protein corona [nm], Effective diameter [nm]
<b>Nominal medium concentration</b>	Initial concentration of NPs in liquid medium [µg/ml]		
<b>Agglomeration</b>	Fractal dimension (2.3), Packing factor (0.637)		
	Single agglomerate [nm]	Agglomerate diameters [nm]	
	Density [g/mL]	Fractions of each agglomerate species [nm]	
<b>Dissolution</b>			Rate constants, Saturated conc. of free ions in solution [µg/mL], Conc. of binding sites available on the proteins per FBS for the fast and slow binding period of the ions [µg/mL %FBS]
<b>Instantaneous cell uptake</b>		Dissociation constant [mol/L]	Thickness of cell membrane [cm], Cell volume [mL], Diffusion coeff. [cm <sup>2</sup> /h]
<b>Time</b>	Time [h] and Time step [s]		
<b>Space</b>	Grid specification (sub-compartment height [nm])		

These models have been integrated into a GUI entirely developed by means of App Designer Tool from MATLAB R2019b (Mathworks) and compiled using MATLAB Compiler. Running the executable file requires MATLAB Runtime, which is free to download from the Mathworks website.

## **Results**

### **A. Opening DosiGUI and running the simulations**

The executable file opens a main window where a brief description of DG, ISDD and ISD3 is provided (Fig. 2).

**DG model description**

The one-dimensional Distorted Grid (DG) model developed by DeLoid et al. (2015) considers the simultaneous tracking of the size distribution of polydisperse particles. The dissolution kinetics is not modeled as a particle surface area limited mechanism nor is it validated against any experimental data. Instead the dissolution is simply modeled as a reduction in agglomerate size in proportion to the extent of dissolution

**ISDD model description**

In vitro Sedimentation, Diffusion and Dosimetry (ISDD) model is developed by Hinderliter and co-workers (2010). It applies well established, long-used principles of diffusional and gravitational transport of particles in viscous media to calculate the movement of particles and their agglomerates from the media to the bottom of a vessel where cells reside.

**ISD3 model description**

In vitro Sedimentation, Diffusion, Dissolution, and Dosimetry model (ISD3) is developed by Thomas et al. (2018) as a general modeling framework for soluble particles, adaptable to a wide range of experimental conditions, particle types, and approaches to describing sedimentation and dissolution. Dissolution can also be turned off, rendering a model like ISDD (Hinderliter et al., 2010) which can also handle spatial distributions of particles, as one might find in larger test systems, like those used in ecological testing. ISD3 models diffusion, sedimentation and cellular uptake of both nanoparticles and dissolved ions: ISD3 assumes nanoparticles instantaneously taken up by cells when reaching their surface (conversely, DG model simulates nanoparticle/agglomerates "accumulation"), while cell uptake of ions is explicitly modeled as a membrane diffusion process. The modular nature of ISD3 also allows the use of different boundary conditions. For example, instead of the instantaneous particle uptake boundary condition, other boundary conditions can also be implemented, such as, no-flux and reactive boundary conditions.

UNIVERSITÀ DI PISA

Research Center E. Piaggio  
University of Pisa

PATROLS  
Advanced Tools for NanoSafety Testing

INFO

**Fig. 2: Main panel of DosiGUI.**

Once the model is initiated by clicking on the *Start* button, the user can manually enter all inputs needed for running the simulations. Alternatively, a pop-up menu (Fig. 3) allows the input parameters to be either directly loaded from a specific file containing the information needed for the chosen model (*Load from file*) or obtained by automatic rearrangement of the input file stored for another model (in Fig. 3 *Load DG simulation*), making it suitable for all the three models. Thus, the same experimental configuration can be simulated exploiting each of the computational frameworks available within DosiGUI, and the consistency of their predictions with measured dose profiles can be tested and compared by means of goodness of fit.

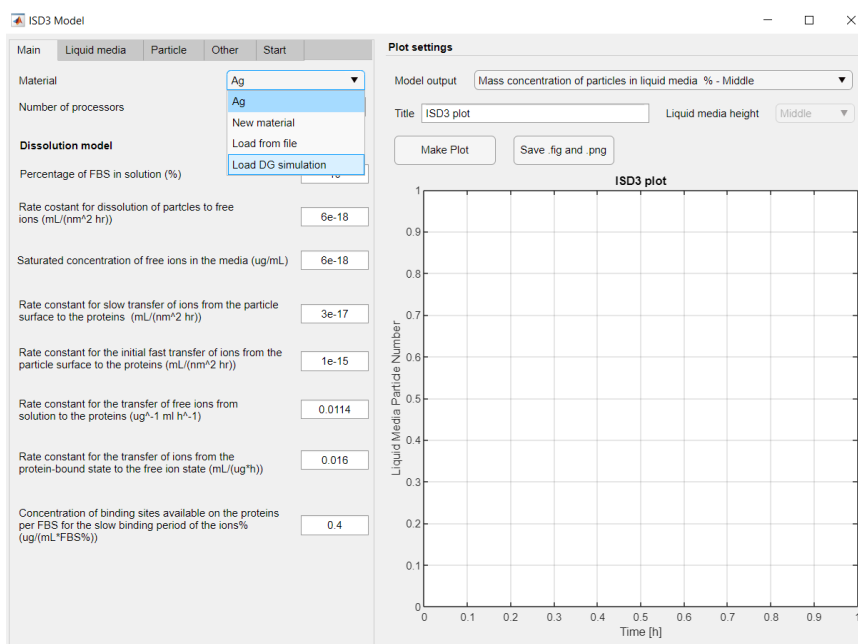


*Fig. 3: Pop-up menu for selecting the loading mode of input data.*

As an example, Fig. 4 shows the interface panel for ISD3 and all categories of the inputs required by this model, including liquid medium and NP parameters (left side). The input values shown in this figure have been experimentally validated in [8]. Specific plot settings are also listed on the right. A loading bar shows the current status of the simulation; then, when the simulation is completed, inputs and outputs are saved into .xlsx and .mat files. The predicted concentrations can be plotted as a function of time or space and the generated figures can be saved as .png, .jpg, .tif or .pdf file.

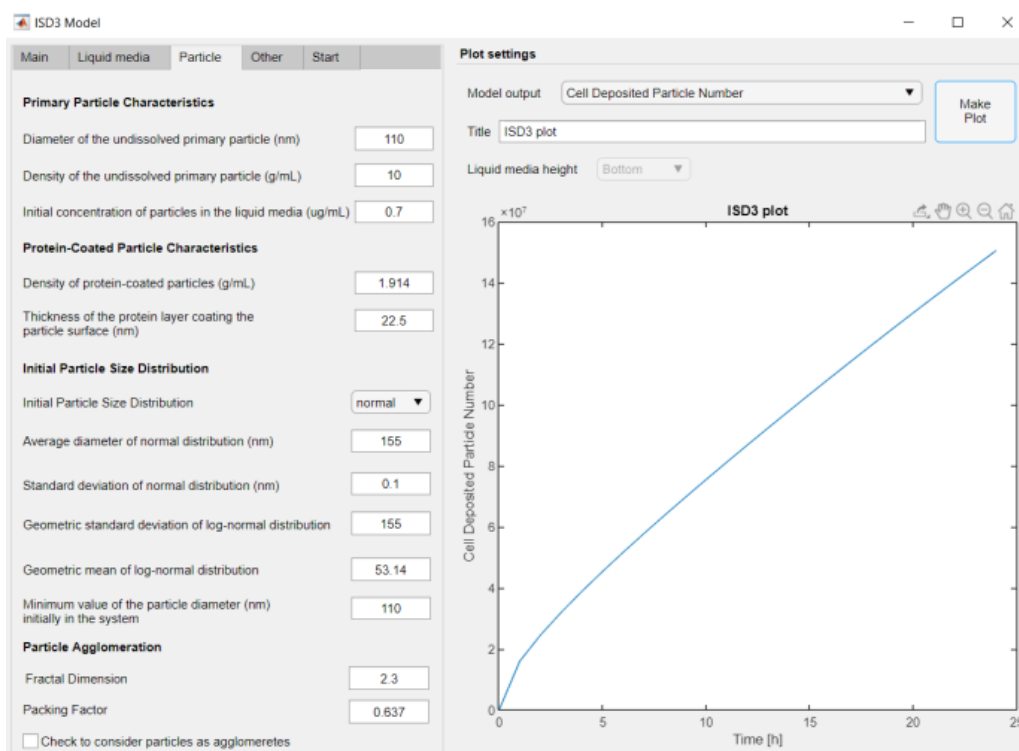


*Fig. 4: Input parameters defining NP properties (left) and plot settings (right).*

All calculations performed by the model are at last summarized and saved into a .txt file named *logfile*. The rationale is to better understand possible interruptions caused by computational errors occurring during the simulation process.

The block diagram in Fig. 5 briefly describes the workflow for the usage of DosiGUI. It is provided as a schematic user guide, with the aim of fully and easily exploiting its functionalities. DosiGUI is available on the PATROLS server ([link](#)) and will be made public once the results on the validation of NP sedimentation currently ongoing at UNIPI and ISTECS are published.

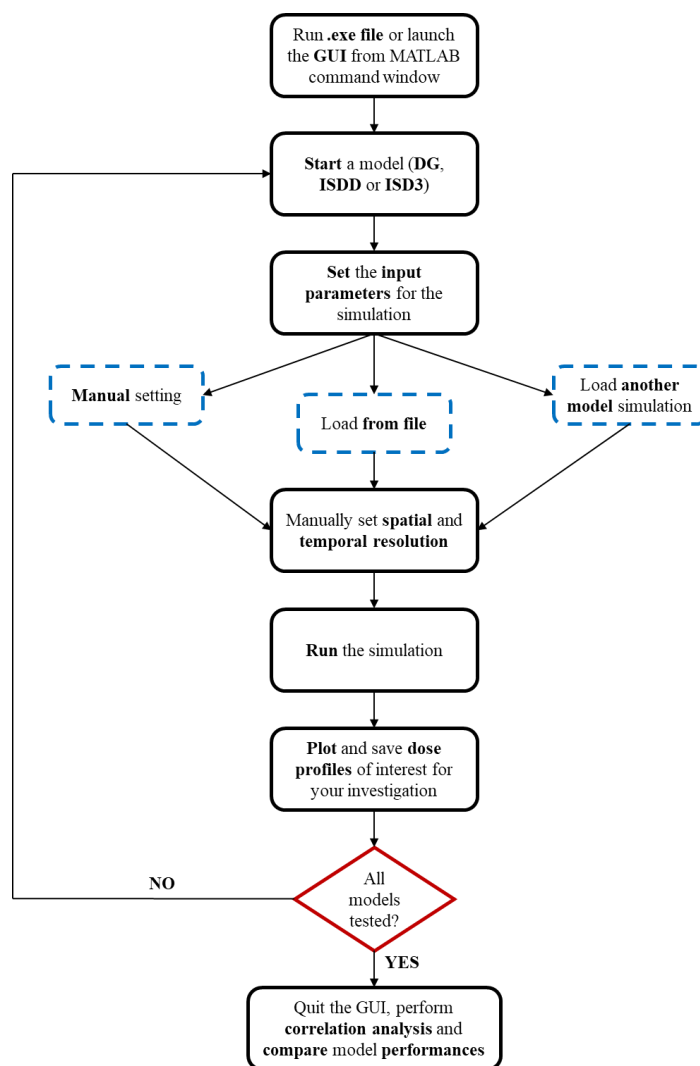


*Fig. 5: Workflow for the usage of DosiGUI.*

## B. Dosimetry of silver NPs

An integrated *in vitro-in silico* approach proposed by UNIPi combines ISD3 [8] with well-established experimental procedures for assessing cytotoxicity [5], providing a more accurate dose-response analysis by reporting nanotoxicity effects as a function of the NP concentrations effectively delivered to cultures (*i.e.* target cell doses) [10]. The study was recently published and is available on the project portal so is only briefly described here [10].

Silver NP characteristics were manually input into ISD3, also specifying the liquid medium parameters (*i.e.* dish depth, volume of medium, temperature, water viscosity and density of medium).

A dose-response curve with the viability of cultured cells (measured via Alamar reagent after 24 h of culture) with respect to the computed target cell doses is shown in Fig. 6. Predicted

target cell doses were around 85% lower than the nominal medium concentrations because of NP transport (*e.g.* NP settling in static experiments, Brownian motion) and dissolution in liquid. The data were used to validate the computational performance of DosiGUI comparing the predicted doses provided by ISD3 with the NP concentrations measured by means of static cuvette experiments performed in duplicate. Strong correlation (*i.e.* Pearson Correlation equal to 0.9991) between computed and experimental concentrations using both DosiGUI and the original source code provided by Thomas et al. [8] confirmed the GUI's precision as well as the ISD3 model's accuracy in simulating NP dynamics in liquid media.

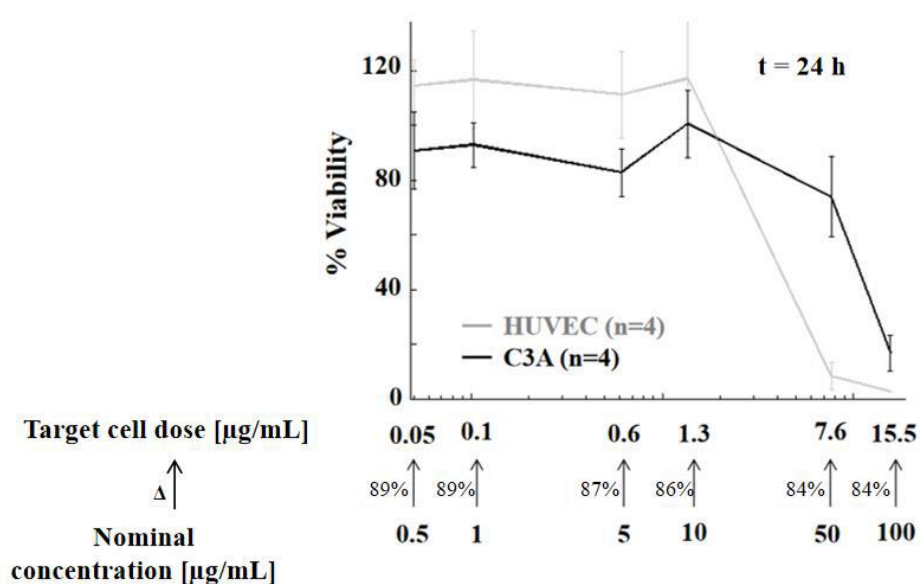


**Fig. 6:** Human Umbilical Vein Endothelial Cells (HUVECs) and human hepatoma-derived immortalized hepatocyte C3A cells cultured in triplicate in 96 well plates showed a decrease of the cell viability with increasing target silver doses reaching the cultures (adapted from [10]). The results were obtained using Thomas' original source code and DosiGUI.

### C. Dosimetry of insoluble NPs

The capability of DosiGUI in supporting the choice of the most suitable of the three models for a specific nanodosimetry application is currently being assessed. The experimental work is being undertaken by ISTEC and will be described fully in WP 1 deliverables. Briefly, Dr. Costa's group measures data on the dynamics of insoluble engineered nanomaterials (*i.e.* CeO<sub>2</sub>, TiO<sub>2</sub> and BaSO<sub>4</sub>), starting from different administered doses (5, 25 and 50 µg/mL) and obtaining middle height concentration over time by dynamic light scattering. In the first set of experiments, the base of the container was coated with a thin gelatin layer to mimic the

adsorption features of a generic cell monolayer. Using DosiGUI, each of the three sedimentation models was evaluated for goodness of fit on the data through correlation analysis. The ISD3 model led to the best fitting ( $R^2 > 0.75$  for all nanomaterials, Tab. 3), so it was used to predict the cumulative effective dose reaching cells over time for each configuration studied (Fig.7).

**Table 3:** Fitting of ISD3 model predictions to the corresponding experimental data.

Nanomaterial	Goodness of fit ( $R^2$ )
TiO <sub>2</sub>	0.83
BaSO <sub>4</sub>	0.76
CeO <sub>2</sub>	0.81

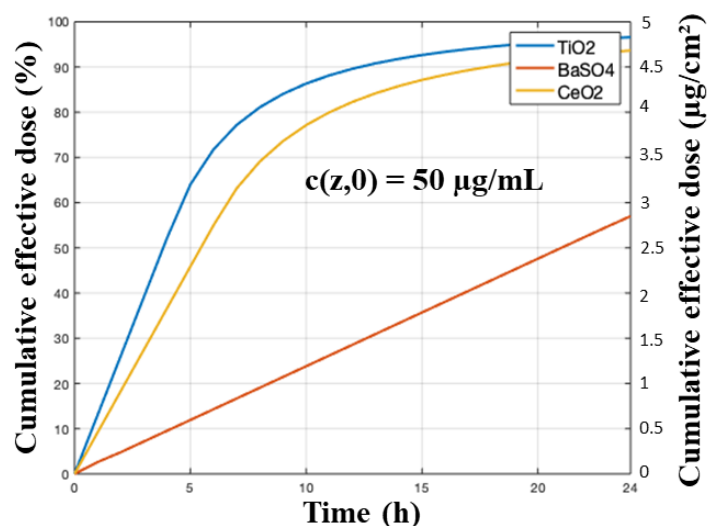


**Fig. 7:** Cumulative effective dose over time predicted by ISD3 for each considered nanomaterial, expressed as percentage of the initially administered dose  $c(z,0)$  (left axis) or as mass of NPs per surface unit (right axis).

Further *in vitro* testing will allow relating this cumulative effective dose with its biological effects, obtaining the dose-response curve. Additionally, for a more exhaustive validation of the tool, the same analysis on insoluble NPs will be performed without the gelatin coating on the set-up bottom, thus reproducing a no flux boundary condition.

#### D. Preliminary considerations about dosimetry on three-dimensional (3D) surfaces

As previously highlighted, the models handled by DosiGUI are 1D: only the vertical axis is considered, and NP deposition is assumed to be homogeneous at the bottom of the domain under consideration (*i.e.* the bottom is a flat and its plane has the same properties in all directions).

As there is some interest in spheroids and 3D models in PATROLS, an assessment of the limitations of the homogenous bottom assumption in terms of NP dosimetry is being made. The first of these uses geometrical considerations to evaluate the actual target dose of NPs at different heights and times, mapping these onto a hypothetical surface with different local heights.

The results suggest that the topology of the surface does have an impact on the target dose. In particular, after 24 h the investigated configuration (sedimentation, diffusion and dissolution of silver NPs in a 3 mm high well, with an initially administered concentration of  $0.7 \mu\text{g/mL}$ ) shows a decrease in target dose of about 7 % from a height of  $300 \mu\text{m}$  to the bottom of the well (Fig. 8A). Such a gradient gradually disappears while moving towards the steady state (*i.e.* 96 h), tending to a uniform surface distribution (Fig 8B). However, since the culture medium is daily refreshed *in vitro*, the latter does not represent an experimentally relevant condition.

The relevance of these considerations to real *in vitro* scenarios will be discussed within the consortium and, if deemed necessary, efforts may be to experimentally measure NP concentrations in a localised manner on surfaces with different geometries.

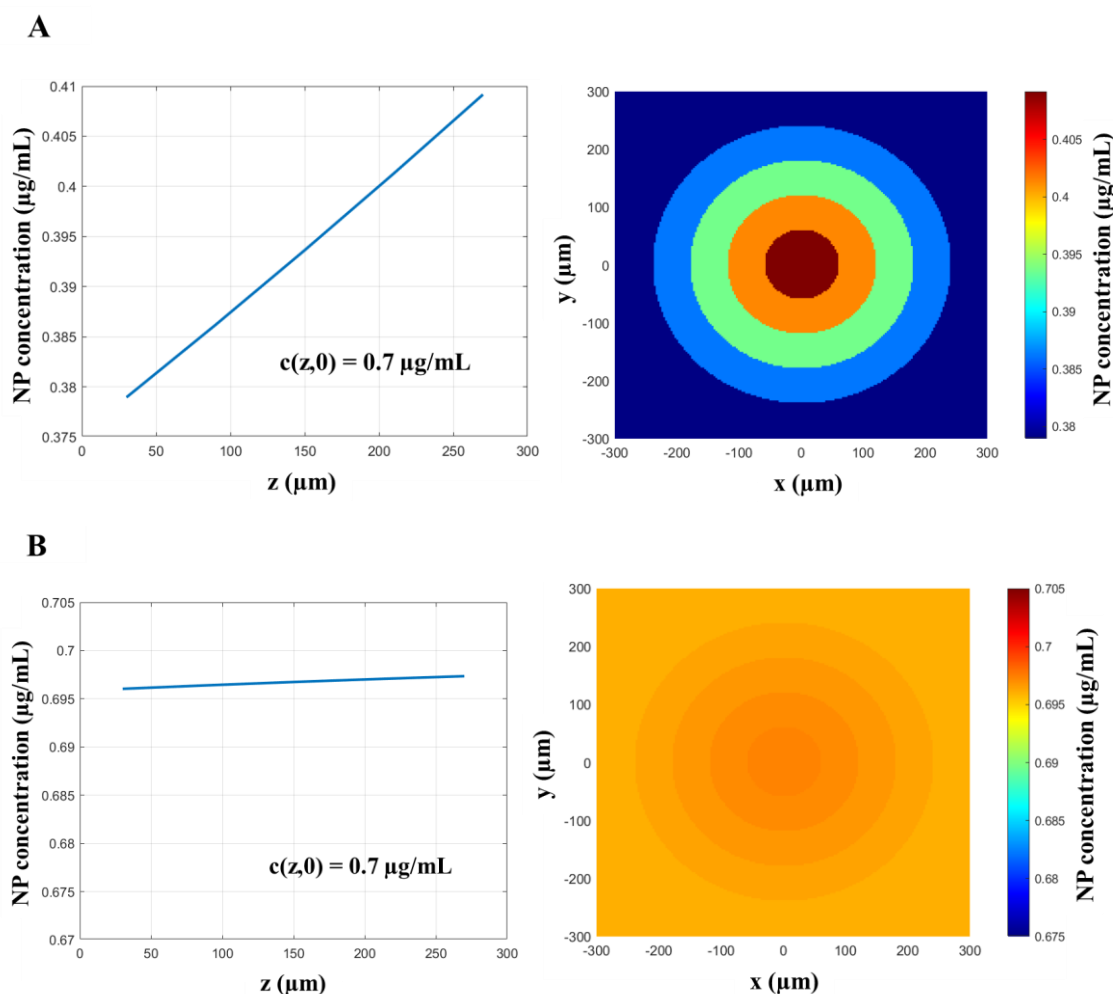


**Fig. 8:** Axial profile (left) and projected surface distribution (right) of silver NP concentration: A) after 24 h of sedimentation dynamics; B) when the steady state of sedimentation processes is reached. Predictions performed for a hypothetical hemispheroidal surface of radius  $300 \mu\text{m}$  by running ISD3 within DosiGUI.

## 2.4 *in vitro* kinetics model

### Introduction

In FP7 SUN a kinetics model describing the dose-response in simple *in vitro* models. The model describes the distribution of the deposited dose into the *in vitro* cell population. IOM will further adapt this model for the more sophisticated *in vitro* models developed in PATROLS. In T1.4, *in vitro* experiments on A549 cells to monitor material uptake, intracellular fate and translocation across the cellular membrane were performed. The ENM used in the experiments were: TiO<sub>2</sub> (NM105), DQ12 (NM200), ZnO (NM110), BaSO<sub>4</sub> (NM220) and CeO<sub>2</sub> (NM212). Two sets of experiments were conducted. The dosing regimen is summarized in Fig 9.

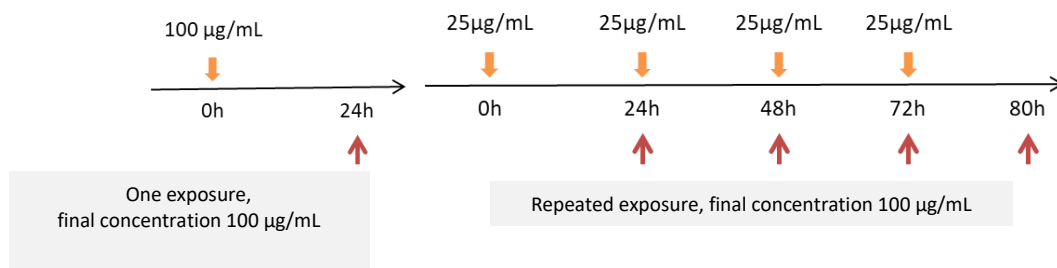


**Fig.9:** The dosing regimen in the one exposure and repeated exposure experiments

The fraction of ENM were measured in the different compartments described in Fig 10.

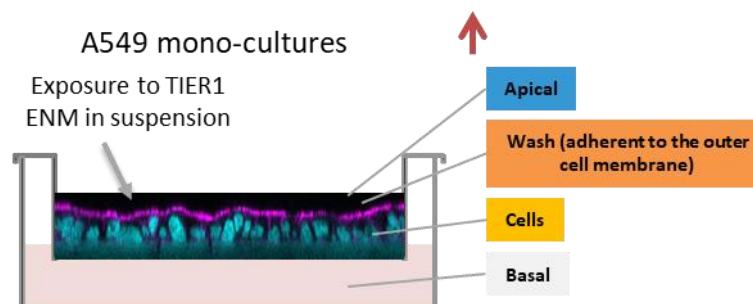


**Fig 10** The different compartments where fraction of deposited dose were measured: (1) Apical, (2) Wash, (3) Cells and (4) Basal.

## Materials and Methods

The model is adapted to simulate the data obtained from T1.4. The model consists of four compartments Apical (A), Wash (W), Cells (C) and Basal (B). The kinetics of ENM translocation in each compartment are described by a series of differential equations:

$$dA/dt = -k_0Adt$$

$$dW/dt = k_0Adt - k_1Wdt \quad (2)$$

$$dC/dt = k_1Wdt - k_2Cdt$$

$$dB/dt = k_2Cdt$$

The model is summarised in Fig 11.

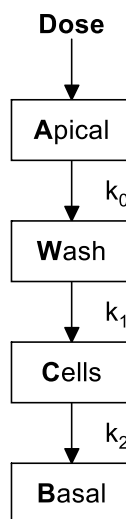


**Fig 11** The kinetics model and the parameters  $k_i$ .

The parameters  $k_i$  ( $i=0,1,2$ ) were estimated using non-linear least squares using the dataset from the first experiment for each ENM. Mathematically, the  $k_i$  were chosen to minimise the sum of squares of the model simulated values, at time=24, for A, W, etc...and their experimental values at the same time.

The model is written in MATLAB and the numerical routine ‘*fmincon*’ of the MATLAB statistical toolbox was used for minimisation in this exercise.

1. The model is calibrated using the dataset of experiment 1 in which a dose of 100  $\mu\text{g/mL}$  is applied at time zero and measurements were made at  $t=24\text{hrs}$  to obtain the parameters.

2. The model is calibrated again using the second experiment for the first 24hr (when a dose of 25  $\mu\text{g}/\text{mL}$  is administered at  $t=0$ ) and the parameters estimated again because the parameters are likely to be dependent on the initial mass dose.
3. The model is then used to simulate the outcomes at 48, 72 and 80 hr for model validation.

## Results

The results of (1) have demonstrated that the kinetics of ENM deposition *in vitro* can be described by a series of linear differential equations. Fig 12 shows the model simulations and the experimental data at  $t=24\text{hr}$  for each of the ENM.

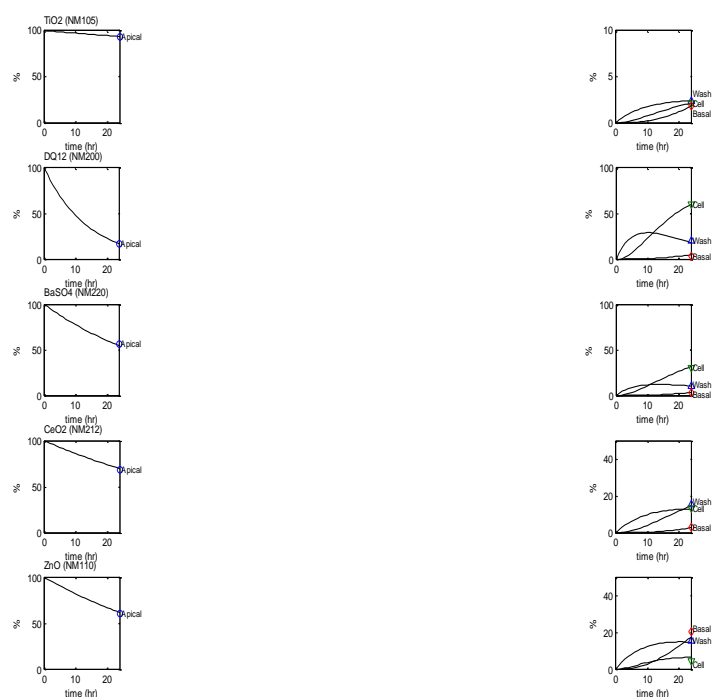


**Fig 12** Model simulation of the single dose (100  $\mu\text{g}/\text{mL}$ ) experiment

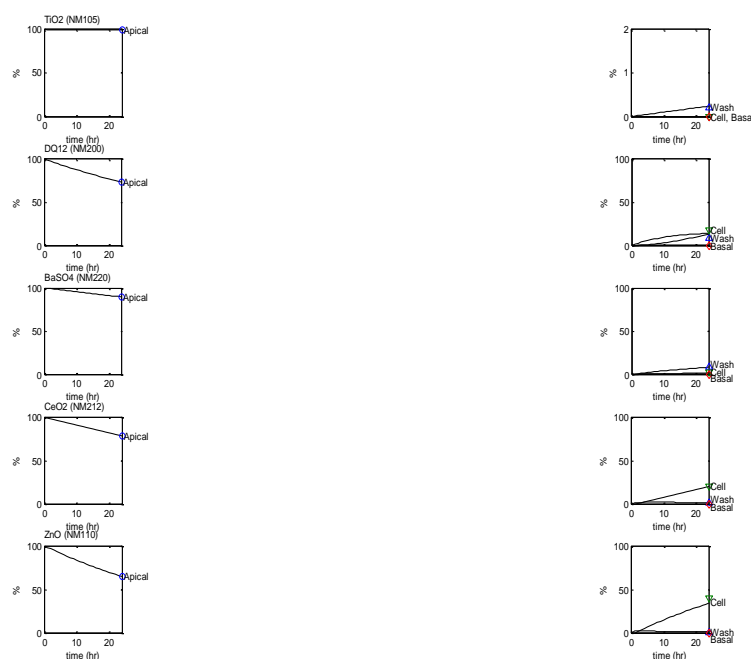
As shown in Fig 12, the model simulation obtained almost perfect fit to the data and therefore have demonstrated that it is suitable for modelling this type of data.

The estimated parameters for ENM are given in Table 4.

**Table 4.** The estimated parameters for each ENM.

	<b>TiO2</b>	<b>DQ12</b>	<b>BaSO4</b>	<b>CeO2</b>	<b>ZnO</b>
<b>k<sub>0</sub></b>	0.003	0.071	0.025	0.015	0.020
<b>k<sub>1</sub></b>	0.1	0.12	0.15	0.08	0.09
<b>k<sub>2</sub></b>	0.08	0.07	0.01	0.02	0.2

For the repeated dose experiment, the results from the first 24hr were used to calibrate the model. The results are shown in Fig 13 and the estimated parameters are shown in Table 5.

**Fig 13.** The model simulation and the results at 24hr when 25  $\mu\text{g/mL}$  was given at  $t=0$ **Table 5** The estimated parameters corresponding to the simulation of Fig 13

	<b>TiO2</b>	<b>DQ12</b>	<b>BaSO4</b>	<b>CeO2</b>	<b>ZnO</b>
<b>k<sub>0</sub></b>	0.0003	0.013	0.0045	0.010	0.018
<b>k<sub>1</sub></b>	0.1	0.06	0.02	0.5	0.9
<b>k<sub>2</sub></b>	0.08	0.02	0.01	0	0

The calibrated model is used to simulate the outcomes when ENM were administered at 24, 48 and 72hr. In each of the dosing the Apical compartment is removed then replaced before dosing. The model prediction and the actual values are compared in Fig 14.

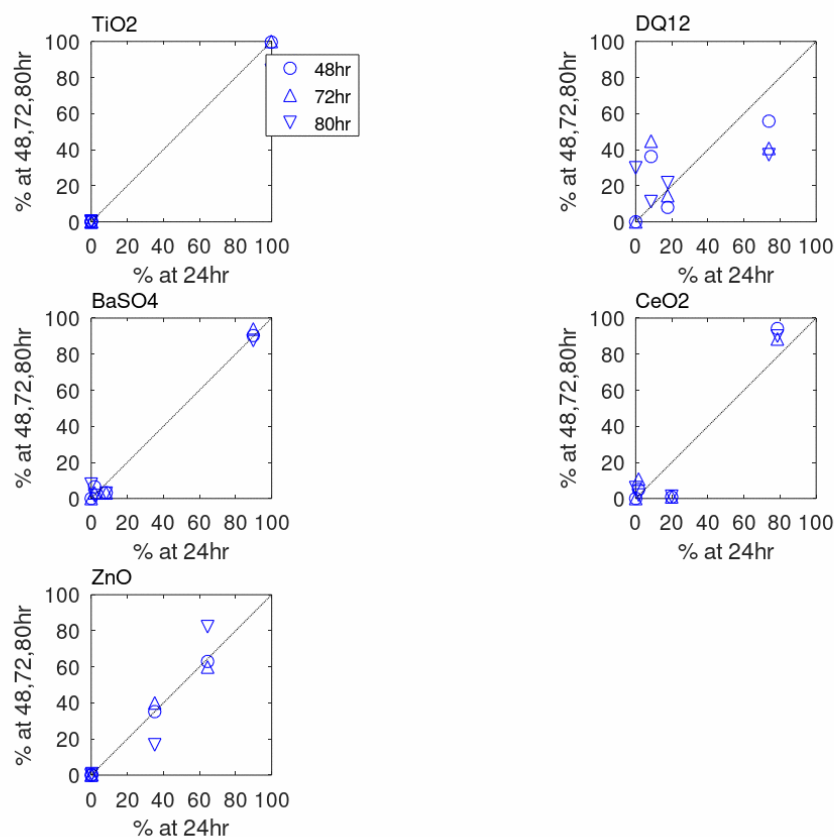


**Fig 14** Model prediction and actual data for all the compartments in the repeated dose experiments.

The model performed relatively well in predicting the outcomes of the repeated dose experiments. Although there are variations in kinetics between the single dose experiment and the first 24hr of the repeated dose experiment when 25  $\mu\text{g/mL}$  was delivered. This is likely to be due the diffusion of the ENM in the Apical compartment which may be dependent on the mass dose administered.

### Estimation of dosing regimen for *in vitro* experiments

T6.2 also delivered a dosing regimen for each ENM to be used in different *in vitro* experiments. The dosing regimen were based on data from the peer-reviewed literature. In this section, the results are summarised for different ENM. The rationale used in choosing the dose regimen is to consider not only *in vitro* data but also *in vivo* equivalent with a view to establish a *in vitro/in vivo* comparison.

### Dose regimen for DQ12, TiO<sub>2</sub>, BaSO<sub>4</sub> and CeO<sub>2</sub>

Monteiller *et al* (2007) [1], used DQ12 in their *in vitro* experiments for a range of NPs. In Figure 15, the dose is described in cm<sup>2</sup>/cm<sup>2</sup> (i.e. cm<sup>2</sup> of dose per cm<sup>2</sup> of well's surface).

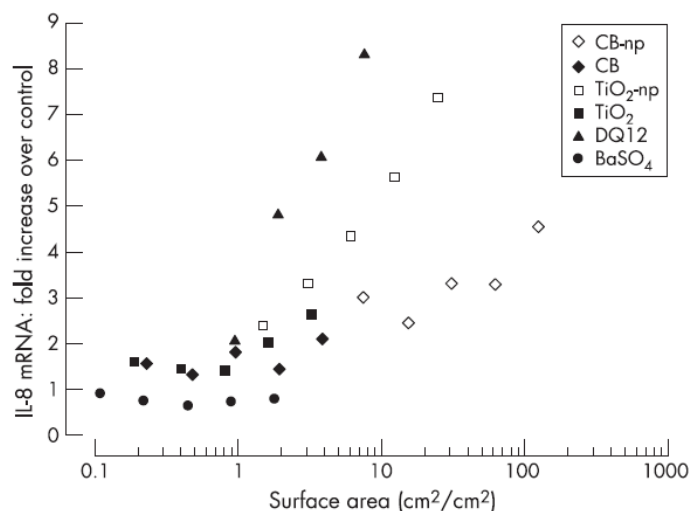


**Fig 15.** IL-8 response from A549 cells to a range of doses for a panel of insoluble particles and NPs

The dose range for DQ12 (from Fig 15) is 0 to 10 cm<sup>2</sup>/cm<sup>2</sup> or 0 to 100 µg/cm<sup>2</sup>. Thus, the *in vitro* dose range should be from 0 to 1 µg/cm<sup>2</sup>. Similarly,

For BaSO<sub>4</sub>, we can derive the dose-range for BaSO<sub>4</sub> is 0-6 µg/cm<sup>2</sup>.

For CeO<sub>2</sub>, the *in vitro* dose-range was chosen to be 0-9 µg/cm<sup>2</sup>.

For TiO<sub>2</sub>, the *in vitro* TiO<sub>2</sub> dose-range is 0-5.2 µg/cm<sup>2</sup>.

For MWCNT, the current estimation of the MWCNT dose range for Mitsui-7 is based on the paper of Chortarea *et al* (2017) [2]. The authors used a range of doses: 0, 5, 10 and 20 µg/mL of Mitsui-7 for 48 hrs exposure and double the dose at 96 hrs for epithelial (A549), macrophage (THP-1) and fibroblast (MRC-5) cell lines separately.

For pro-inflammatory assays, IL-1β and IL-8 are expressed in THP-1 mainly (at both 48 and 96 hrs). The level of IL-1β is no different from control in MRC-5 cells and IL-8 is not significantly higher than control.

For pro-fibrotic assays, PD-GF, OPN and TGF-β are measured. For cell proliferation, BrDU is used and assessed semi-quantitatively in MRC-5. Increased TGF-β and OPN release was demonstrated in Mitsui-7-treated fibroblasts only in the 96 hrs exposure. Interestingly, no

proliferation was observed in MWCNT exposed MRC-5 cells and consequently no increase in collagen production was observed.

Similarly, elevated PD-GF and a slight increase in TGF- $\beta$  were observed after 96 hours of Mitsui-7 exposure in THP-1 cells. Also, Mitsui-7 were found to significantly increase TGF- $\beta$  and PD-GF secretion into the supernatant of exposed epithelial cells after 96 hours.

For the combined, multi cell type *in vitro* system, much depends on the seeding of each cell type and the rate of 'interstitialisation'. Thus, if dosing is from the 'alveolar' side, it is challenging to get up to 20  $\mu\text{g/mL}$  into the fibroblast cell below. Therefore, the dose (at 48 and 96 hrs) is in such a way that would deliver enough TGF-b or PD-GF from A549/THP-1 to the fibroblasts below (the indirect effect) and, at higher doses, to get enough MWCNT to stimulate fibroblasts directly. Since a high dose, 150  $\mu\text{g/mL}$ , has been used in the past. we suggest a dose-range for Mitsui-7 in our experiment as follows:

0, 5, 10, 20, 40 and 80  $\mu\text{g/mL}$  at 48 hrs and double that for 96 hrs. Thus, the highest dose, at 96 hrs, will be 160  $\mu\text{g/mL}$ : close to the dose quoted in the paper. The dose range suggested may generated enough pro-fibrosis release that would stimulate fibroblasts to proliferate and produce collagens without the direct dose effect which hinders fibroblast proliferation as suggested in the paper.

*For silver ENM*, we determined the dose range for an *in vitro* dose-response experiment with silver NPs. The determination is based on the published results of Xu et al (2013), Choo et al (2017) [3,4]. From Xu et al (2013), a clear dose-response, with respect to cell viability (for murine peritoneal macrophages) , was observed for a dose-range of [0 to 100  $\mu\text{g/mL}$ ], after 24hr exposure to silver NPs.

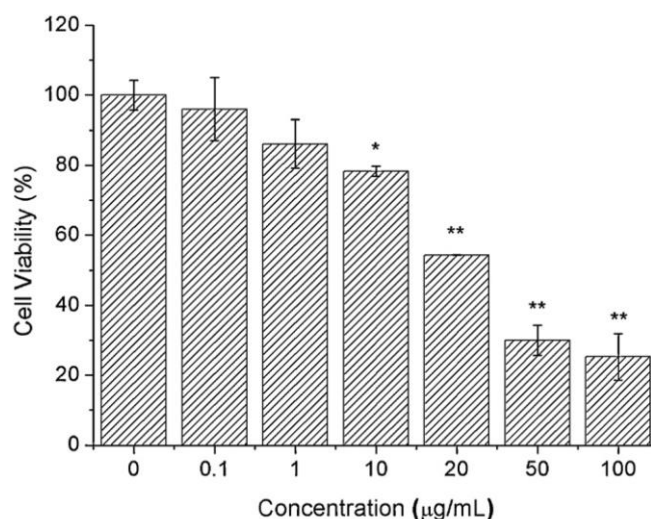


**Fig 16.** The viability of murine peritoneal macrophages after 24hr exposure to silver NPs.

The authors noted that the cell viability significantly decreased at 10 µg/mL. When the dose is increased to 20 µg/mL the cell viability is reduced significantly to 54 percent. Therefore 10 µg/mL is chosen to be the dose for moderate toxicity. The doses which elicit cytokine release are bound to be lower than this critical dose. Choo et al (2017) assessed the viability of the Balb/c 3T3 A31-1-1 (fibroblast) cell line at 72 hr using a dose range of [0 to 10.6 µL]. Their results are summarised in Table 6.

**Table 6.** Cytotoxicity of silver NPs with respect to 2 assays: Crystal Violet (CV) and Colony formation (CFE).

AgNPs (µg/mL)	CV	CFE
NOAEC	2.65	-
IC <sub>50</sub>	5.91	0.17
IC <sub>90</sub>	9.59	9.34

The No Observed Adverse Effect Concentration (NOAEC) is estimated at 2.65 µg/mL and the IC<sub>50</sub> is at 5.91 µg/mL (much less than the results of Xu et al above). For the purpose of our experiment, we need to:

1. Do a cell viability assay to identify the IC<sub>50</sub> and NOAC, then
2. Increase dose in an increment of 0.5 µg/mL, from 0 µg/mL until the IC<sub>50</sub> then the IC<sub>90</sub>.  
For example, at 72 hr, assuming the NOAEC to be at 2.65 and IC<sub>50</sub> at 5.91, the dose

range would be [0, 0.5, 1, 1.5, 2, 2.5 (near the NOAEC), 3, 3.5, 4.5, 5, 5.5, 6 (near the IC<sub>50</sub>), 9.5 (near IC<sub>90</sub>)].

The rationale here is to try to capture the time course of the cytokines (e.g. TNF- $\alpha$ , IL-8) which is expected to diminish as the cells become increasingly non-viable.

In the estimation of the dose range for our experiment, we should note also that Xu et al measured their assay at 24 hr while Choo et al at 72 hr and there may be difference in particle size. Also, there is a difference in cell type (peritoneal macrophage versus fibroblast) and the difference in cell viability assays. However, based on their findings, it is possible to sketch a strategy for dosing silver NPs for our experiments. Thus, the following approach was recommended.

1. Do a cell viability assay to identify the IC<sub>50</sub>, IC<sub>90</sub> and NOAEC, measured at 24hr and 72 hr.
2. Then do a dose range from 0, 0.5,..., until the IC<sub>50</sub> then the IC<sub>90</sub> and measure the cytokine release at 24hr and 72 hr.

*For ZnO*, ZnO ENM were used in a wide range of cell lines (e.g. A549, C2C12, HaCaT human keratinocytes, colon cells Caco-2, immune cells: monocytes, macrophages ...). The responses can range from cell viability to Ca<sup>2+</sup> influx, loss of membrane integrity, IL-8 mRNA expression to NF- $\kappa$ B activation.

The dose range for ZnO NP is 0, 5, 10, 25, 50, 100  $\mu$ g/mL in Buerki-Thurnherr et al (2013) [5], cytotoxicity of Jurkat A3 cell line (ATCC, Wesel, Germany, CRL-2570), a human leukemic T cell line) increased from 25  $\mu$ g/mL (40pc cell death approx.) to 100  $\mu$ g/mL (80pc approx.), see Fig 17.

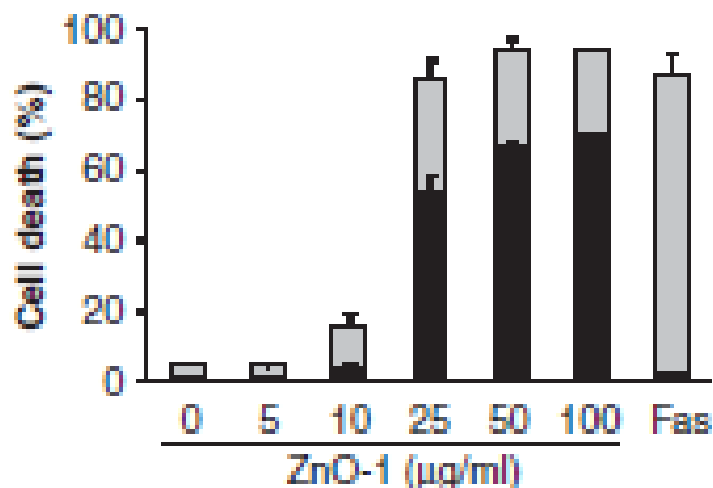


*Fig 17* Dose-Response for ZnO-1 (commercially available from AG, Germany).

Thus, to study sub toxic doses, we should concentrate on the range of 0 to 25 µg/mL., using the following range [0, 5, 10, 15, 25, 30, then 50 and 100] µg/mL. Also note that, because of fast dissolution, measurements the responses at 6hr and 24 hr are also needed.

For the responses the markers of inflammation ((IL-8 expression), Oxidative Stress (Glutathione depression) and markers of fibrosis (collagen production or hydroxyproline) should be measured.

### 3. Deviations from the Workplan

The partners of WP6 and in particular, D6.2 have performed according to the Workplan. There is no significant deviation from the plan. Although the construction of the GUI was originally planned for IOM and Harvard, this is now done by UNIPI.

### 4. Performance of the partners

The partners have performed adequately and delivered according to the description of WP6.

### 5. Conclusions

In D6.2, three types of *in silico* models have been constructed. The QSAR model which establishes a quantitative relationship between the NP physico-characteristics and the response; the Diffusion models which describe the deposition of NP in an *in vitro* system and the dynamics model describing the kinetics of the NP in an *in vitro* model based on data from T1.4. In D6.2 the *in vitro* dose range for several NP is also established and is used in the experimental

studies of the other W., The models of D6.2 will contribute to the analysis of the dose-response data being generated from these WP when they become available.

The Steering Board deems this deliverable to be fulfilled satisfactorily for submission.

## 6. Annex

### References for 2.1

- [1] K. Jagiello, S. Halappanavar, A. Rybinska-Fryca, A. Williams, U. Vogel, T. Puzyn, *Small* **2020** (Minor revision)
- [2] S. S. Poulsen, A. T. Saber, A. Williams, O. Andersen, C. Kobler, R. Atluri, M. E. Pozzebon, S. P. Mucelli, M. Simion, D. Rickerby, A. Mortensen, P. Jackson, Z. O. Kyjovska, K. Molhave, N. R. Jacobsen, K. A. Jensen, C. L. Yauk, H. Wallin, S. Halappanavar, U. Vogel, *Toxicology and Applied Pharmacology* **2015**, 284, 16.
- [3] S. S. Poulsen, N. R. Jacobsen, S. Labib, D. Wu, M. Husain, A. Williams, J.P. Bogelund, O. Andersen, C. Kobler, K. Molhave, Z. O. Kyjovska, A. T. Saber, H. Wallin, C.L. Yauk, U. Vogel, S. Halappanavar, *PLoS One* **2013**, 8, e80452.
- [4] S. Halappanavar, L. Rahman, J. Nikota, S. S. Poulsen, Y. Ding, P. Jackson, H. Wallin, O. Schmid, U. Vogel, A. Williams, *NanoImpact* **2019**, 14, 100158.

### Reference for 2.2

Multiple-Path Particle Dosimetry Model (MPPD v 3.04)

(<https://www.ara.com/products/multiple-path-particle-dosimetry-model-mppd-v-304>).

### References for 2.3

- [1] C. Beer, R. Foldbjerg, Y. Hayashi, D. S. Sutherland, and H. Autrup, “Toxicity of silver nanoparticles—Nanoparticle or silver ion?”, *Toxicol. Lett.*, vol. 208, no. 3, pp. 286–292, 2012.
- [2] N. Durán, C. P. Silveira, M. Durán, and D. S. T. Martinez, “Silver nanoparticle protein corona and toxicity: a mini-review,” *J. Nanobiotechnology*, vol. 13, p. 55, Sep. 2015.
- [3] Y. Li, Y. Zhang, and B. Yan, “Nanotoxicity overview: nano-threat to susceptible populations,” *Int. J. Mol. Sci.*, vol. 15, no. 3, pp. 3671–3697, Feb. 2014.
- [4] G. A. Oomen *et al.*, “Grouping and Read-Across Approaches for Risk Assessment of Nanomaterials,” *International Journal of Environmental Research and Public Health*, vol. 12, no. 10. 2015.

- [5] N. Ucciferri *et al.*, “In vitro toxicological screening of nanoparticles on primary human endothelial cells and the role of flow in modulating cell response,” *Nanotoxicology*, vol. 8, no. 6, pp. 697–708, Sep. 2014.
- [6] G. M. DeLoid *et al.*, “Advanced computational modeling for in vitro nanomaterial dosimetry,” *Part. Fibre Toxicol.*, vol. 12, no. 1, p. 32, 2015.
- [7] P. M. Hinderliter *et al.*, “ISDD: A computational model of particle sedimentation, diffusion and target cell dosimetry for in vitro toxicity studies,” *Part. Fibre Toxicol.*, vol. 7, no. 1, p. 36, 2010.
- [8] D. G. Thomas *et al.*, “ISD3: a particokinetic model for predicting the combined effects of particle sedimentation, diffusion and dissolution on cellular dosimetry for in vitro systems,” *Part. Fibre Toxicol.*, vol. 15, no. 1, p. 6, 2018.
- [9] L. Böhmert *et al.*, “In vitro nanoparticle dosimetry for adherent growing cell monolayers covering bottom and lateral walls,” *Part. Fibre Toxicol.*, vol. 15, no. 1, p. 42, 2018.
- [10] Poli, D., Mattei, G., Ucciferri, N. *et al.* An Integrated *In Vitro–In Silico* Approach for Silver Nanoparticle Dosimetry in Cell Cultures. *Ann Biomed Eng* **48**, 1271–1280 (2020). <https://doi.org/10.1007/s10439-020-02449-5>

#### **References for 2.4**

- [1] Monteiller et al (2007). The pro-inflammatory effects of low-toxicity low-solubility particles, nanoparticles and fine particles, on epithelial cells in vitro: the role of surface area. *Occup Environ Med* 2007;64:609–615. doi: 10.1136/oem.2005.024802
- [2] Chortarea et al (2017). Profibrotic Activity of Multiwalled Carbon Nanotubes Upon Prolonged Exposures in Different Human Lung Cell Types. *Applied In Vitro Toxicology* Vol. 5, No. 1.
- [3] Xu et al (2013), Evaluation of the adjuvant effect of silver nanoparticles both in vitro and in vivo. *Toxicology Letters* 219 (2013) 42– 48.
- [4] Choo et al (2017). Morphological transformation induced by silver nanoparticles in a Balb/c 3T3 A31-1-1 mouse cell model to evaluate *in vitro* carcinogenic potential. *Env Health and Toxicol.* Volume: 32, Article ID: e2017016, 8 pages.
- [5] Buerki-Thurnherr, T et al (2013). *In vitro* mechanistic study towards a better understanding of ZnO nanoparticle toxicity. *Nanotoxicology*, 7:4, 402-416.

